Mechanical properties and grain orientation evolution of zirconium diboride-zirconium carbide ceramics

D'Angio', Andrea; Zou, Ji; Binner, Jon; Ma, Hai-Bin; Hilmas, Gregory E.; Fahrenholtz, William G.

DOI:
10.1016/j.jeurceramsoc.2017.09.013

Mechanical properties and grain orientation evolution of zirconium diboride-zirconium carbide ceramics

A. D'Angio'[a,*], J. Zou[a *], J. Binner[a], Hai-Bin Ma[b], G.E. Hilmas[c] and W.G. Fahrenholtz[c]

[a] *School of Metallurgy and Materials, University of Birmingham, Birmingham, UK*

[b] *Shanghai Institute of Ceramics, Chinese Academy of Science, Shanghai, China*

[c] *Materials Science and Engineering Department, Missouri University of Science and Technology, Rolla, MO, USA*

Abstract

The effect of ZrC on the mechanical response of ZrB_2 ceramics has been evaluated from room temperature to 2000°C. Zirconium diboride ceramics containing 10 vol% ZrC had higher strengths at all temperatures compared to previous reports for nominally pure ZrB_2. The addition of ZrC also increased fracture toughness from ~3.5 MPa $\sqrt{m}$ for nominally pure ZrB_2 to ~4.3 MPa $\sqrt{m}$ due to residual thermal stresses. The toughness was comparable with ZrB_2 up to 1600°C, but increased to 4.6 MPa $\sqrt{m}$ at 1800°C and 2000°C. The increased toughness above 1600°C was attributed to plasticity in the ZrC at elevated temperatures. Electron back-scattered diffraction analysis showed strong orientation of the ZrC grains along the [001] direction in the tensile region of specimens tested at 2000°C, a phenomenon that has not been observed previously for fast fracture (crosshead displacement rate = 4.0 mm min^{-1}) in four point bending. It is believed that microstructural changes and plasticity at elevated temperature were the mechanisms behind the ultrafast reorientation of ZrC.

Keywords: ultra-high temperature ceramics (UHTC); particulate reinforced composites; borides; high-temperature mechanical properties; electron backscattering diffraction (EBSD);

1. Introduction

Ultra-High Temperature Ceramics (UHTCs) are candidate materials for sharp leading edges, nose caps and flight control components of aerospace vehicles that can operate at hypersonic speeds [1-4]. These components are exposed to extreme environments that include temperatures exceeding 2000°C, heat fluxes of hundreds of W/cm^2 and intensive chemical aggression by dissociated air [5].

* Corresponding authors: Dr. Ji Zou, j.zou@bham.ac.uk; Andrea D'Angio' axd322@bham.ac.uk

Amongst the UHTCs, zirconium diboride (ZrB_2) has excellent mechanical properties, high thermal conductivity and reasonable chemical resistance [6-8]. Its high electrical conductivity also permits electrical discharge machining and, hence, the fabrication of complex shapes [9]. However, ZrB_2 suffers from low sinterability [10, 11] and requires the use of sintering aids. Additions of disilicides ($MoSi_2$, $TaSi_2$, $ZrSi_2$) have been used to improve the densification of ZrB_2 [12-16], but the resultant ceramics are limited in terms of their potential structural applications because of their lower melting points. Boron carbide (B_4C) and silicon carbide (SiC) are also commonly added to ZrB_2 [17-20], but the formation of eutectic products below 2500°C remains an issue [21]. As well as improving the sinterability, the addition of second phases has also been explored to increase strength and fracture toughness [19, 22]. Additions of 30 vol% silicon carbide in a ZrB_2 matrix have shown a nearly 50% increase in the toughness [10]. Chamberlain *et al.* [23] reported that the room temperature bend strength of ZrB_2-30 vol% SiC attrition milled with tungsten carbide (WC) media exceeded 1 GPa and the fracture toughness peaked at 5.3 MPa$\sqrt{m}$. Zou et al. [24] added 5 vol% WC to a ZrB_2-20 vol% SiC composite, which retained a strength of 600 MPa up to 1600°C whereas ZrB_2-20 vol% SiC without WC did not .

Zirconium carbide (ZrC) additions to ZrB_2 are beneficial for both densification and mechanical properties at elevated temperatures. As observed by Gropyanov *et al.* [25], 10 wt% ZrC in ZrB_2 reduced the porosity of the host material to less than 1% after hot pressing at ~1900°C with a decrease in the activation energy for densification from ~774 kJ mol^{-1} to ~527 kcal mol^{-1}. The addition of the second phase also promoted grain boundary pinning, which reduced grain size in the final ceramic. In a study of the bending creep of ZrB_2-ZrC and TiB_2-TiC [26], additions of 20 wt% ZrC reduced the porosity from ~10% to ~3% and the grain size from 6-8 μm to 2-4 μm after hot-pressing at 2100°C. More recently, spark-plasma sintering at 1800°C produced ZrB_2-ZrC with as little as ~2.5% residual porosity [27].

Characterization of mechanical behaviour of ZrC-ZrB_2 at elevated temperature has focused on creep behaviour [26] and comparing it to the creep of ZrC [28-34]. In the ZrC-ZrB_2 system, creep has been measured for ZrC contents from 20 to 70 mol%. The creep rates of the ZrB_2-ZrC ceramics exceeded those of the individual constituents by two orders of magnitude. This superplastic behaviour correlated with the self-diffusion of carbon in ZrC [29-31, 35, 36] and has been extended to other carbides with the same crystal structure as ZrC [37-42]. Relatively few papers have explored the strength of either single-phase ZrC [33, 34]

or ZrB_2-ZrC at temperatures above 1500°C [43]. Neuman *et al.* [43] investigated the strength, flexural strength and fracture toughness of ZrB_2-10 vol% ZrC from room temperature to 2300°C and concluded that the observed increase in toughness in the range 1600-2000°C resulted from plasticity of the ZrC.

The present work focused on microstructure-mechanical property relationships for ZrB_2-10 vol% ZrC ceramics from room temperature to 2000°C to determine the mechanism by which the ZrC additions enhanced mechanical behaviour.

2. Materials and methods

2.1. Materials

ZrB_2 and ZrC powders (both Grade B, H.C. Starck, Karlsruhe, Germany) together with ZrH_2 (Grade S, Chemetall, Jackson, Michigan) were suspended in methyl ethyl ketone using 0.4 wt% of a dispersant (DISPERBYK®-110, BYK-Gardner, Columbia, Maryland). The slurry was ball milled for 4 h at 60 rpm in a polypropylene container using home-made ZrB_2 milling media to minimize contamination[†]. The powder:milling media ratio was 2:1 by volume. Phenolic resin (GP 2074, Georgia Pacific, Atlanta, Georgia) was added to the slurry as a carbon precursor (the char yield was ~43 wt% at 800°C in a Ar/10H_2 atmosphere). Carbon reacts with and removes surface oxides from the powders and any residual carbon could react with ZrH_2 to form additional ZrC. The slurry was ball milled for another 20 hours, thus totalling 24 hours. The mixture was subsequently dried by rotary evaporation (Rotavapor R-124, Buchi, Flawil, Germany) at ~80°C and a rotation speed of 80 rpm. Once dried, the powders were sieved through a 60 mesh screen and uniaxially pre-pressed at ~2.4 MPa and then hot-pressed (Model HP50-7010G, Thermal Technology, Santa Rosa, California) in 63.5 mm square graphite dies lined with two boron nitride-coated layers of graphite foil having an individual thickness of ~125 μm (2010-A , Mineral Seal Corp., Tucson, Arizona).

[†]Milling media were prepared from ZrB_2 powder with additions of 1 wt% B_4C and 1 wt% C; homogeneity of the additions was achieved via ball-milling using WC-6Co balls (Note: ~1 wt% WC was added to the powder through erosion). The mixture was uniaxially pressed into beads and then cold isostatically pressed. Finally, media were pressurelessly sintered at 2050°C for 90 min in flowing Ar/H_2.

The first stage of hot pressing involved pyrolysys of the phenolic resin via heating the green body under flowing Ar/10H_2 at 5°C/min up to 800°C and holding for 1 h. Subsequently, the furnace was evacuated to ~20 Pa and the temperature was increased to 1250°C with a heating rate of 10°C/min. The temperature was held for 2 hours and then further increased to 1450°C by again heating at 10°C/min. Following another 2 h hold at 1450°C, the temperature was increased to 1600°C. After a 1 h hold at 1600°C, the furnace was backfilled to ~10^5 Pa with Ar/10H_2 and a uniaxial pressure of 32 MPa was applied. The holds at 1250°C, 1450°C, and 1600°C were used to promote removal of oxide impurities such as boria and zirconia by vaporization and/or reaction with carbon, as reported in previous studies [17, 18]. The furnace was finally heated up to 1900°C by heating at 20°C/min. A final hold of 45 minutes was performed and then the chamber was cooled down with an average rate of 20°C/min. The pressure was removed at 1600°C.

2.2. Characterisation

Hot pressed billets were sliced and then polished using successively finer diamond colloidal suspensions with a final abrasive size of 0.25 μm. Polished sections were etched at 100°C for 20 s using 2.0 molar KOH solution. The microstructure was characterized using a field emission gun scanning electron microscope, FEGSEM (JSM 7000F, JEOL USA Inc., Peabody, Massachusetts) equipped with an energy-dispersive X-Ray spectrometer (EDS Oxford) and wavelength-dispersive X-Ray spectrometer (WDS Oxford) for chemical analysis. The grain sizes of the ZrB_2 and ZrC and the amount of the two phases were determined by computerized image analysis by counting at least 200 grains (ImageJ software, National Institutes of Health, Bethesda, Maryland). For higher resolution observation and nanoscale analysis a transmission electron microscope (JEOL 2100F, JEOL USA Inc., Peabody, Massachusetts) was used.

X-Ray diffraction (XRD) and grazing incidence X-ray diffraction (GIXRD) (X'Pert^3 MRD, PANalytical B.V., Almelo, The Netherlands) were used for the characterisation of the crystalline phases in as-sintered materials and specimens broken at elevated temperatures. ICDD Cards no. 34-0423 and 74-1221 were used to identify respectively ZrB_2 and ZrC.
Cross sections of bars broken in 4-point bending at 1800°C and 2000°C were analysed using electron back scattered diffraction (EBSD) analysis on a Quanta 3D FEGSEM (Hillsboro, Oregon) equipped with a EBSD detector (NordLysNano, Oxford Instruments, Abingdon, United Kingdom). Data were analysed using the software *CHANNEL* 5 (HKL Technology,

Denmark). Specimens were polished using the same procedure outlined above, but with a final polish using a 40 nm colloidal silica suspension (OPS, Struers ApS, Ballerup, Denmark). The same analysis was also carried out on a specimen that had not been broken as a reference. The EBSD scans were performed with a step size of 0.5 μm. The acquired Kikuchi patterns were indexed automatically by selecting the space group $Fm\bar{3}m$ for ZrC [44] and P6/mmm for ZrB_2 [10] The overall texturing was expressed in multiples of uniform density (MUD) which varied from 1 (random orientation) to infinity (perfectly oriented single crystal). A coordinate frame *xyz* was defined as follows: the *z* direction was parallel to the bending stress axis, whereas *x* and *y* determined the plane of the cross section of the specimen.

2.3. Mechanical testing at room temperature

Flexural strength was tested in 4-point bending using a fully articulated fixture and B type bars specimens were used (45 x 4 x 3 mm) according to ASTM C1161. The bars were machined from hot-pressed billets by diamond grinding (600 grit) on a surface grinder (FSG-3A818, Chevalier, Santa Fe Springs, California). The tensile surfaces were then polished to a 1 μm finish using diamond slurries. Ten specimens were tested at room temperature in a screw-driven load frame (Model 33R4204, Instron, Norwood, Massachussets). The crosshead displacement rate was 0.5 mm min^{-1}.

Toughness was measured by the chevron notch beam method using B bars (45 x 4 x 3 mm) in 4-point bending according to ASTM C1421. The notch was obtained using a dicing saw (Accu-cut 5200, Aremco products, Ossining, New York) with an ~150 μm-thick diamond blade. The notch dimensions were measured after testing using a digital microscope (KH-3000, Hirox-USA, Hackensack, New Jersey) and 5 specimens were tested at room temperature. The crosshead displacement rate was 0.05 mm min^{-1}.

Young's modulus was determined both from the slope of the load-displacement curves (ASTM E411) and by dynamic measurements according to ASTM E1876.

2.4. Mechanical testing at elevated temperature

Flexural strengths were measured at 1000°C, 1400°C, 1600°C, 1800°C and 2000°C according to ASTM C1211 using the same size bars as the room temperature specimens. The tests were performed using an induction heater (SI30KWLF, Superior Induction Technology,

Pasadena, California) with a graphite susceptor. The system was enclosed in an environmental chamber with a flowing argon atmosphere around the test fixture [45]. The specimens were loaded and secured by cyanoacrylate glue in the fully articulated four-point bending fixture [46]. The specimen was heated up to test temperature with a rate of 50°C/min and held for 5 minutes to permit temperature equilibration of the specimen and fixtures. Crosshead displacement rate was varied with temperature to maintain a linear elastic response to rupture with the rates summarized in Table 2. The reported strength was the average of five measurements at each tempertaure. Fracture toughness was tested at the same elevated temperatures and in the same chamber as flexural strength. The reported values of fracture toughness were the average of three measurements.

3. Results and discussion

The theoretical density was calculated based on the nominal composition (ZrB_2-10 vol% ZrC) using values of 6.09 g cm^{-3} for the ZrB_2 [10] and 6.56 g cm^{-3} for the ZrC [47]. The resultant value was 6.14 g cm^{-3}, which is consistent with the value determined by geometric density (6.17 g cm^{-3}). The amount of ZrC, as determined by imaging, was 9.9 vol%, with 0.4 vol% amorphous phase. The ZrB_2 had a mean grain size of 4.7 ± 1.6 μm with a maximum size of ~10 μm and an aspect ratio 1.5 ± 0.4, whilst the ZrC grain size was 1.7 ± 0.7 μm with an aspect ratio 1.4 ± 0.3.

The microstructures shown in Figure 1 showed that the ceramics were nearly fully dense and did not contain a significant fraction of pores. A small volume fraction (<0.1 vol%) of pores was observed entrapped within ZrB_2 grains.

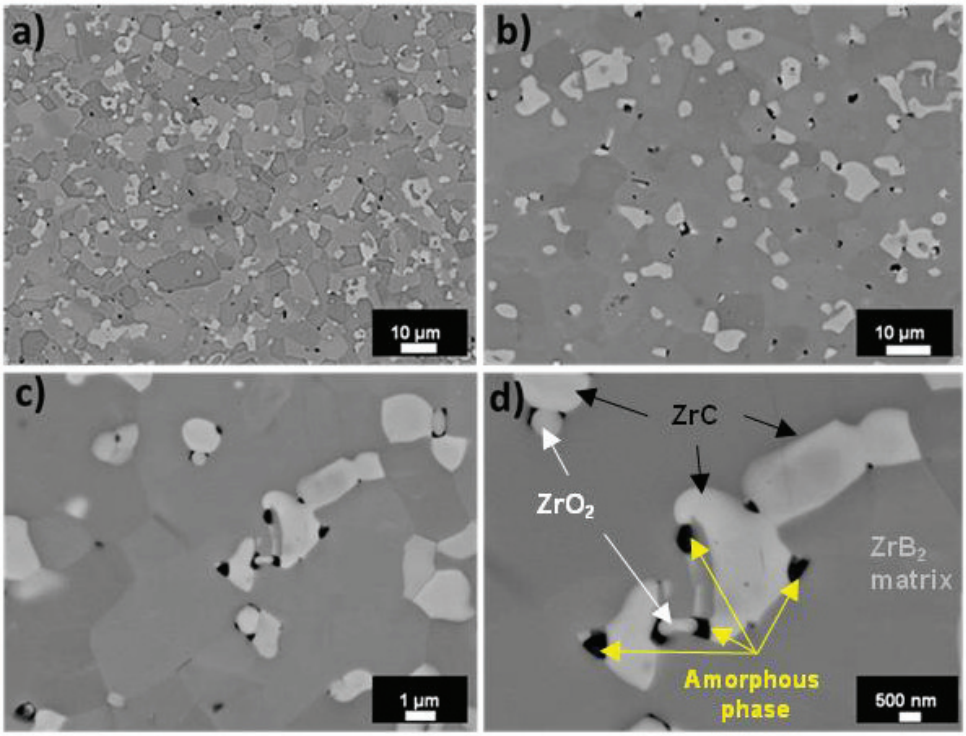

Figure 1.Backscatted-electron micrographs of ZrB_2-ZrC at different magnifications. ZrC grains are in light grey and black spots represent the amorphous phase. c) and d) show clusters of ZrC grains with the amorphous phase.

A residual phase with very dark contrast was also present, which appeared as black spots in the micrographs as indicated by arrows in Figure 1d. This phase was distinguished from pores because of charging observed around the perimeter of pores during imaging. As shown in Figure 2, TEM-EDS revealed the presence of aluminium, silicon, and calcium in the amorphous phase.

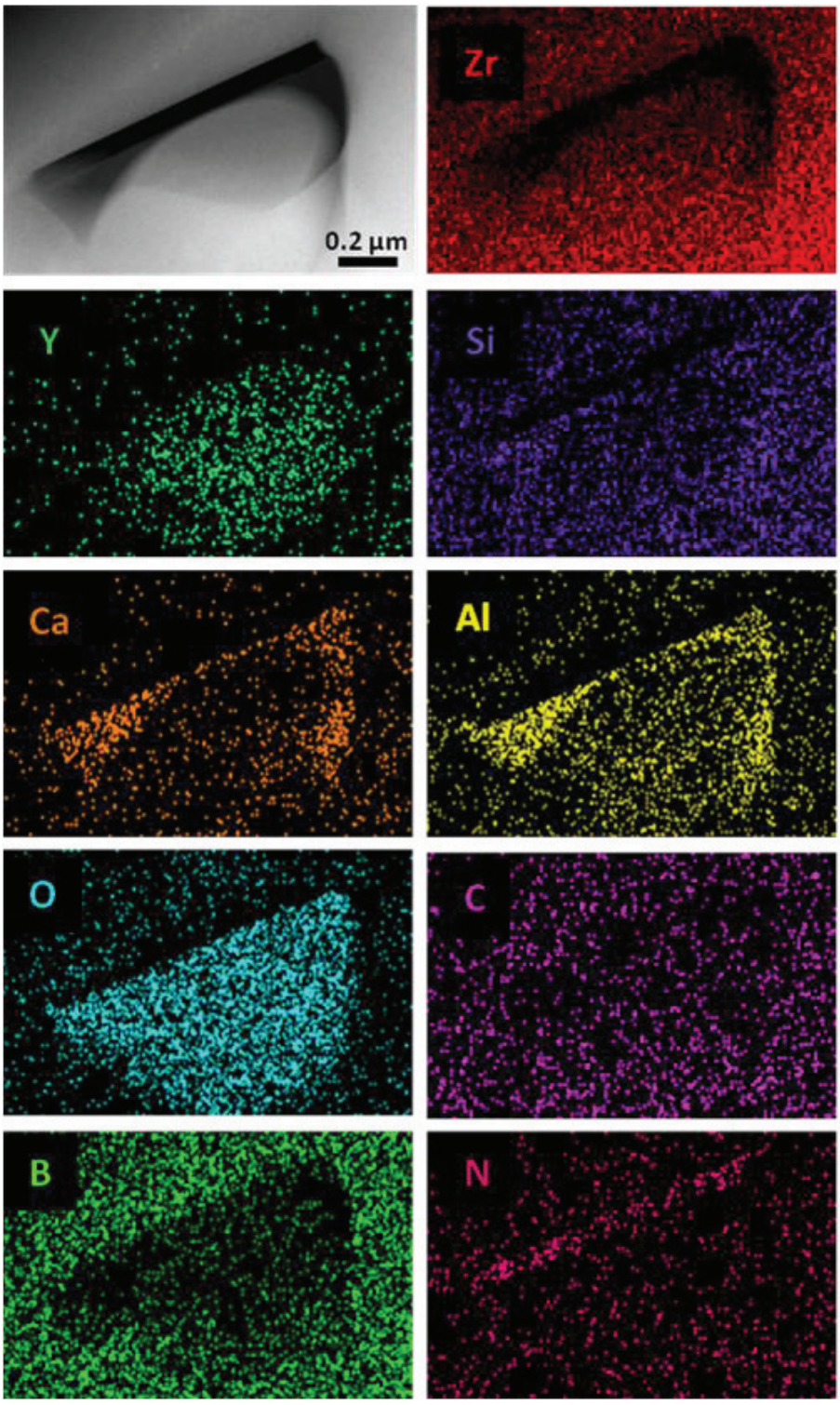

Figure 2. Elemental maps for the distribution of Zr, Y, Si, Al, Ca, C, O, B and N in the amorphous phase.

Submicrometer monoclinic ZrO_2 grains were typically found encapsulated within the amorphous phase (e.g., as shown in Figure 3). The amorphous phase containing zirconia was predominantly found adjacent to ZrC grains. The zirconia particles were likely formed by spontaneous oxidation of ZrC during the reaction of ZrH_2 and carbon at low oxygen activity in the densifying compact. The boron nitride formation may be associated with reaction of

boria with nitrogen impurities contained in the starting powders [48]. As will be discussed later, the presence of the amorphous phase adjacent to the nascent ZrC may play an important role in the mechanical behaviour at elevated temperatures.

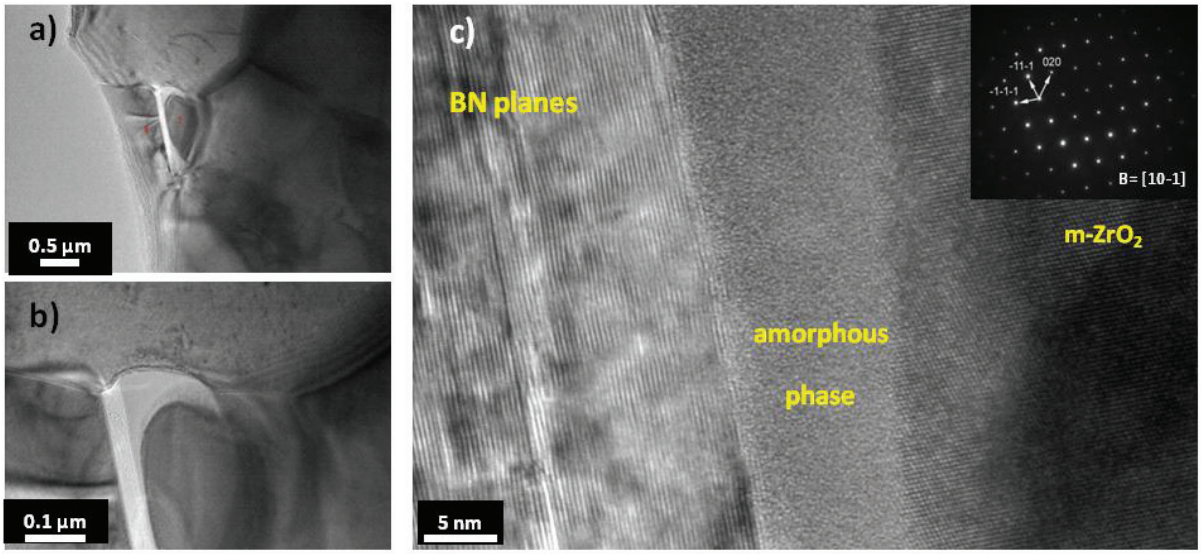

Figure 3. Morphology of the amorphous phase encapsulating monoclinic zirconia grain.

Heating to elevated temperatures for mechanical testing did not result in any changes in the phases present in the test bars. X-ray diffraction patterns shown in Figure **4** showed the same relative amount of zirconia (ICCD card no. 37-1484) compared to the as-sintered material (labelled RT). Note that a logarithmic scale was used to increase the size of low-intensity peaks. Grazing incidence angle X-ray diffraction performed on the tensile surface of test bars revealed that the surface of the specimen broken at 2000°C (labelled GI2000°C) is free from zirconia, but the intensity of ZrC was higher.

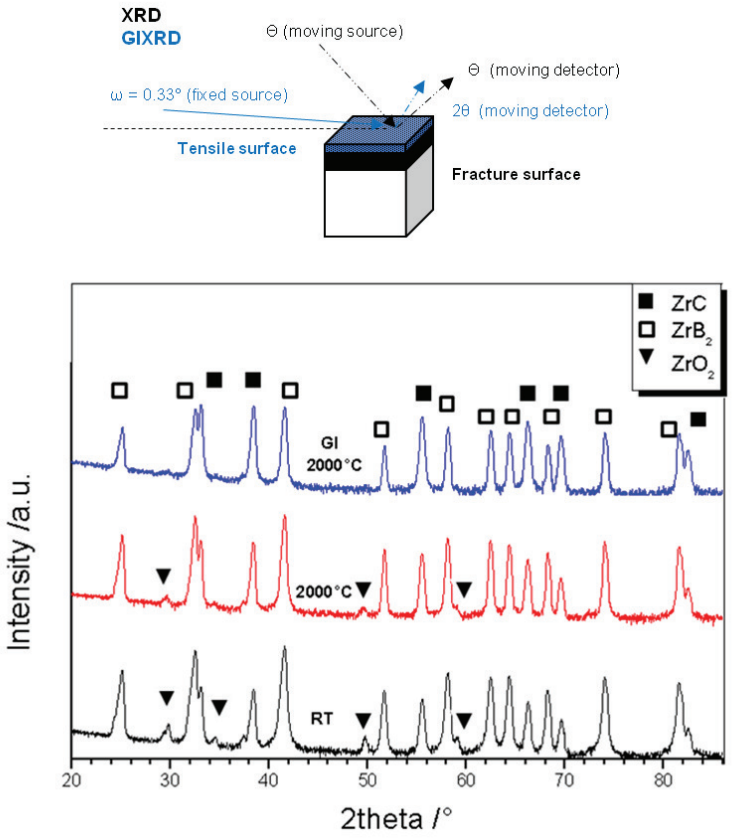

Figure 4. XRD patterns of the as-sintered ZZC10, after mechanical testing at 2000°C and GIXRD of the sample broken at 2000°C.

Fracture surfaces of specimens tested in 4-point bending at room temperature, 1000, 1400, 1600, 1800 and 2000°C are shown in Figure 5. At room temperature (Figure 5a)), ZrB_2 grains exhibited transgranular fracture, whilst failure was intergranular at high temperature (Figure 5b), c), d), e) and f)). The specimens fractured from 1000 to 1600°C showed the formation of a zirconia layer on both the ZrB_2 and ZrC grains.

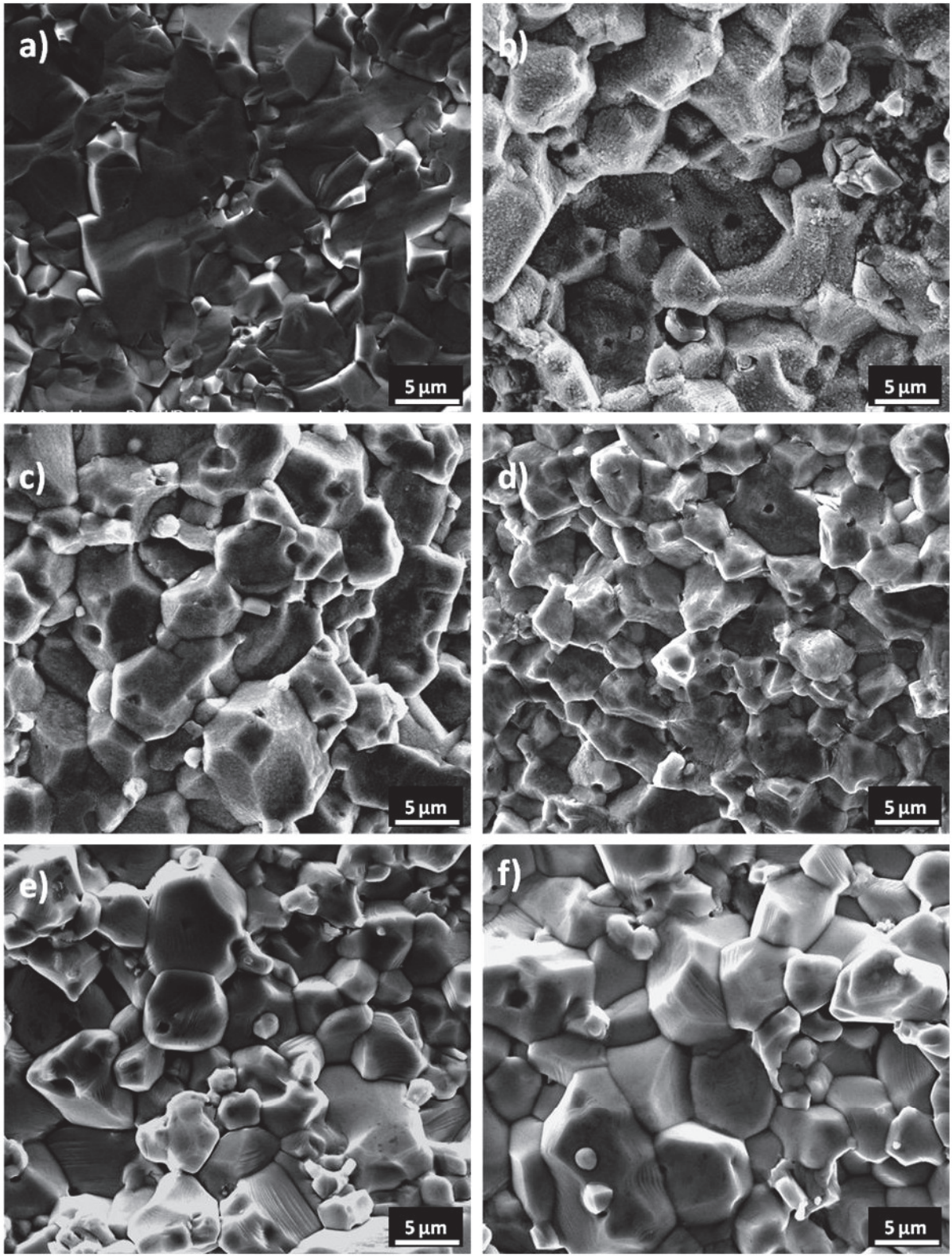

Figure 5. Fracture surfaces of specimens broken at a) room temperature, b) 1000°C, c) 1400°C, d) 1600°C, e) 1800°C and f) 2000°C.

The morphology is shown in detail in Figure 6. At 1800°C and 2000°C, no zirconia was observed on the fracture surfaces. This implied the presence of a transition from an oxidising to inert furnace environment at temperatures between 1600°C and 1800°C. The oxygen

activity in the furnace was previously estimated to be between 10^{-16} and 10^{-14} atm [22]. The observed transition and oxygen activity are consistent with a Zr-O-C volatility diagram reported by Maitre et al. [49]. They calculated that the upper limit of oxygen activity for stability of solid ZrC was 10^{-20} atm at 1327°C and 10^{-17} atm 1527°C. Since the stability domain for ZrC moves to higher oxygen pressures with increasing temperature, it is reasonable that the pO_2 is in the range 10^{-16} - 10^{-14} atm at 1800°C. Moreover, at pO_2 values as low as about 10^{-14} atm, carbon can oxidise in CO-rich atmospheres [50]. At 1527°C, CO partial pressures lower than ~10^{0} atm can reduce ZrO_2. Overall, the thermodynamics suggest that the oxygen partial pressure in the mechanical testing furnace was low enough to inhibit oxidation of the ZrB_2 and ZrC at temperatures of 1800°C or higher. Further, the carbon-rich environment of the induction-heated graphite hot zone may have promoted reduction of any zirconia that was present near the tensile surface. This localised carbothermal reduction may also explain the decrease in the amount of zirconia formed with increasing temperature (**Figure 5** b, c and d) [51, 52].

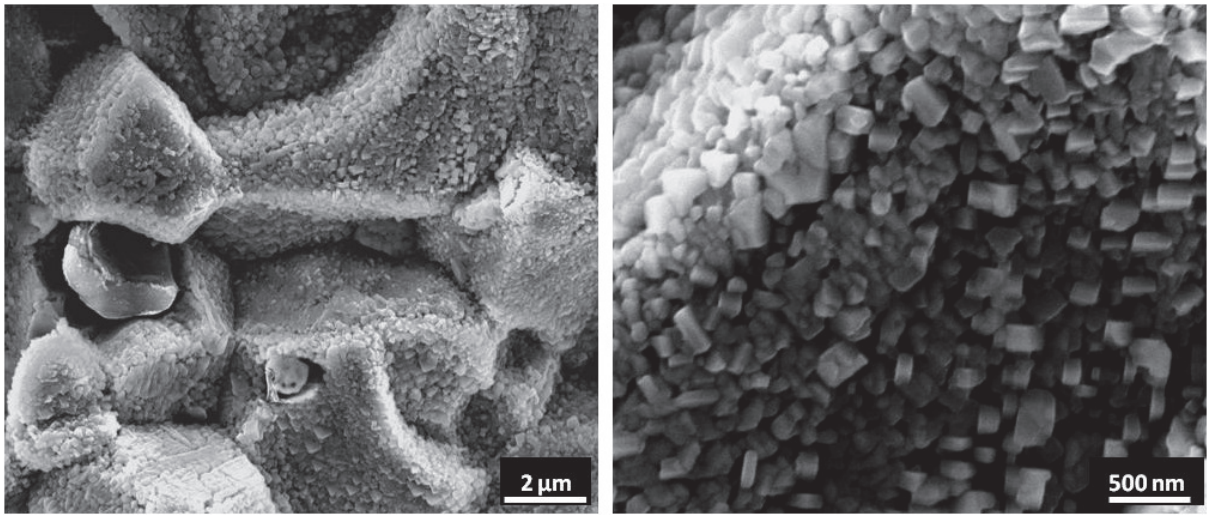

Figure 6. Formation of zirconia layer on the fracture surface of ZZC10 tested at 1000°C.

Specimens fractured at 2000°C exhibited a terraced structure on the surfaces of the grains (Figure **7**). Texturing on fracture surfaces has previously been attributed to minimisation of surface energy [53]. According to Wulff's rule [54, 55], the ratio of specific surface energy (γ_i) to the distance of the crystal faces from a point within the crystal (h_i) is constant. Thus, the crystallographic plane with the lowest γ_i has the lowest h_i, which indicates the lowest crystal growth rate. The crystallographic plane with the lowest γ_i generally corresponds to the highest atomic density. For example, the (111) plane in the ZrC lattice has a higher surface density than other planes such as (001) and (011) and, therefore, a lower γ_i. Hence, for ZrC,

formation of the terraces in the [111] direction should be suppressed, while formation in the [001] direction should be promoted.

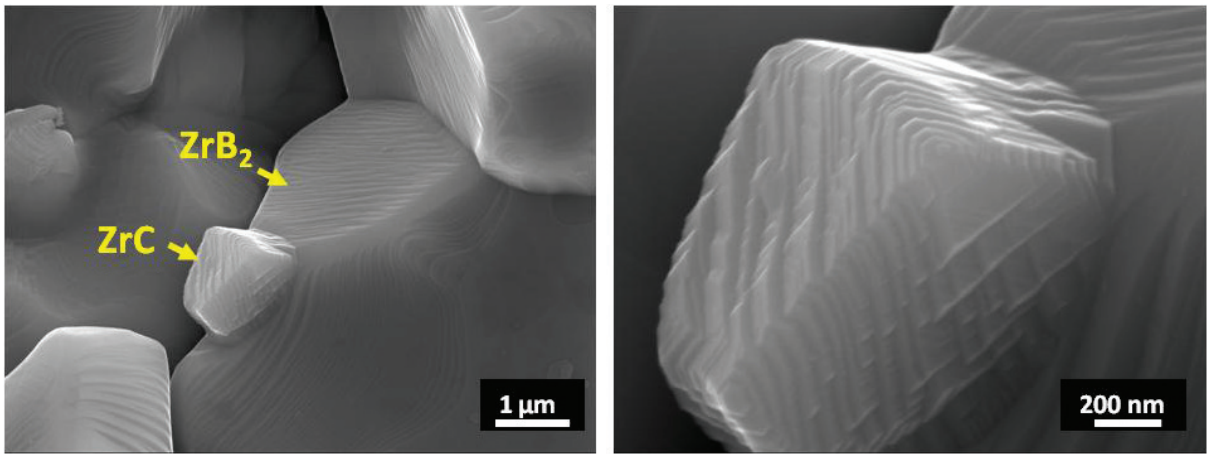

Figure 7. Fracture surface of ZZC10 broken at 2000°C with formation of terraced microstructure.

HRTEM analysis (Figure 8) of a ZrC grain adjacent to amorphous phase confirmed the formation of a faceted surface as well as the crystalline orientations of the facets. The d-spacing of 0.281 ± 0.008 nm corresponded, within the uncertainty of the measurements, to the separation (0.274 nm) of the {111} family of planes in ZrC.

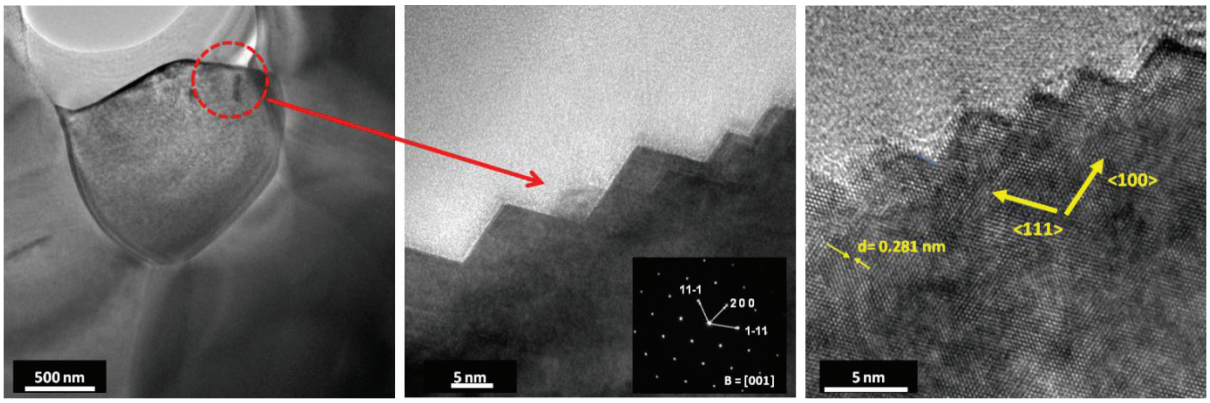

Figure 8. Faceted ZrC grains at the ZrC-amorphous phase interface.

However, it must be noted that at the ZrC-ZrB_2 interface, the grains are not faceted (see Figure 9).

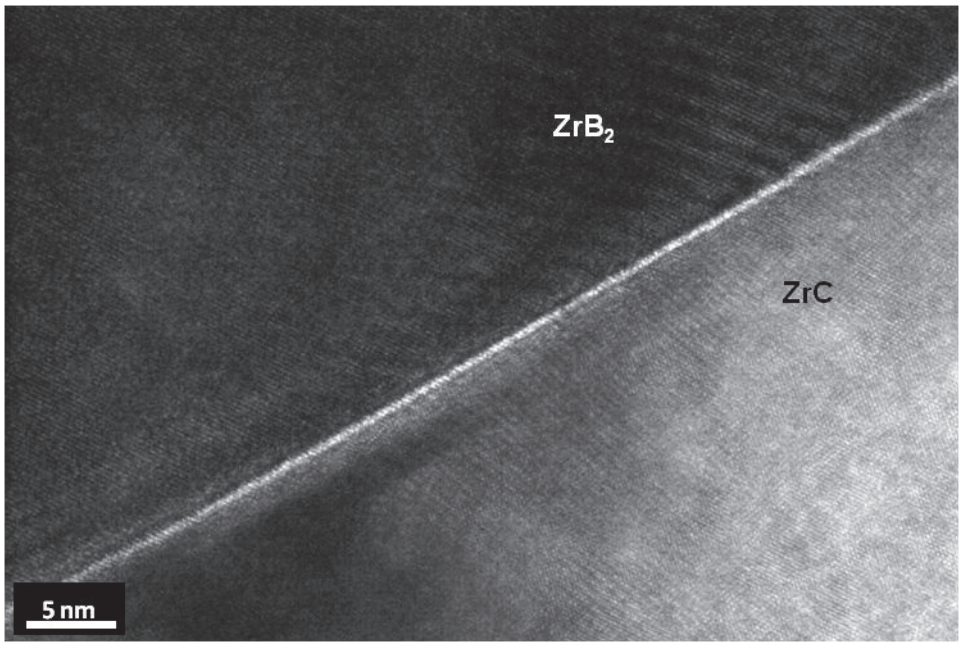

Figure 9. Boundary between ZrB_2 and ZrC grains.

This suggests that the faceted morphology is typical of free surfaces which are either:

i) On the fracture surface; after fracture, the specimen cooled at a rate of 20°C/min. However, this means that the specimen temperature was above 1800°C for 10 min. At these temperatures, both ZrB_2 and ZrC grains on the fracture surface are able to rearrange their crystalline structures.

ii) At the interface with the amorphous phase; at 2000°C, the amorphous phase is viscous and exerts only a marginal constraint on the grains as they evolve towards a faceted morphology.

This microstructural rearrangement in both ZrB_2 and ZrC was triggered at temperatures above 1800°C. Rearrangement occurred at free surfaces such as the fracture surface (Figure 7) and at interfaces with the viscous/molten amorphous phase (Figure 8). For strong interfaces such as those between ZrB_2 and ZrC (Figure 9), the faceted morphology was not observed.

The composition and properties of ZrB_2-ZrC ceramics are reported in Table 1; the room temperature elastic moduli were 525 GPa from static bend testing and 515 GPa from the acoustic method. Both values are in agreement with predictions made using a volumetric rule of mixtures and moduli values for the constituent phases in the range 490-530 GPa for ZrB_2 [10, 11, 56, 57] and 390-460 for ZrC [8, 58, 59]. The flexural strength was 596 MPa, which was more than 50% higher than the strength of ZrB_2 with 0.5 vol% of carbon, labelled as ZB-

0.5C and reported as a reference material [60] in Figure 10. The room temperature fracture toughness value was 4.3 MPa$\sqrt{m}$, which is higher than monolithic ZrB_2 (typically ~3.5 MPa$\sqrt{m}$) [60] and comparable with ZrB_2-SiC composites ceramics [23]. The toughness increase is likely due to the residual stresses that arise due to the differences in the coefficients of thermal expansion for the ZrB_2 matrix and the isolated ZrC particles. An Eshelby analysis [61] of ZrB_2 – ZrC predicts that the stress in the matrix was about 450 MPa assuming that the temperature of stress relaxation was 1400°C, the particulate radius 0.85 μm, the matrix radius 2.35 μm, the coefficient of thermal expansion 6.7 x 10^{-6} K^{-1} [10] for ZrB_2 and 7.5 x 10^{-6} K^{-1} for ZrC [62], the Poisson's ratio 0.133 for ZrB_2 [10] and 0.197 for ZrC [63], and the Young's modulus 520 GPa for ZrB_2 [64] and 450 GPa for ZrC [63]. Based on this analysis, the matrix will be in compression because of the lower CTE of ZrB_2. This compressive stress acting on the matrix may promote the fracture toughness increase of the composite [65] as:

$$\Delta K_{IC} = 2\bar{\sigma}\sqrt{\frac{2(\lambda - 2a)}{\pi}} = 1.19\ MPa\sqrt{m} \quad (1)$$

where a is the particulate radius, $\bar{\sigma}$ is the interfacial pressure and λ is the average interparticulate spacing [66], evaluated as :

$$\lambda = \frac{1.085 \times 2a}{\sqrt{f_p}} = 5.83\ \mu m \quad (2)$$

where f_p is the volume fraction of the particulate.

ZrB_2 with 0.5 vol% C had a toughness at room temperature of 2.9 MPa$\sqrt{m}$, but with the addition of ZrC, the value increased to 4.3 MPa$\sqrt{m}$. The estimated residual stresses are highly influenced by CTE mismatch and reported CTE values for ZrC vary from ~7 to above 8x10^{-6} K^{-1}[62, 67-70]. Overall, the addition of ZrC to the ZrB_2 matrix enhanced the flexure strength and fracture toughness because of the CTE difference between the constituents.

The flexure strength and fracture toughness at elevated temperature are summarized in Table 2. Figure 10 shows the flexural strength and fracture toughness as a function of testing temperature. Strength did not vary significantly between room temperature and 1000°C, but decreased to about 330 MPa by 1800°C and then maintained roughly that strength up to 2000°C. The drop in strength above 1000°C has been observed for a number of carbides and borides [38, 71-74] and is likely due to the relaxation of thermal residual stresses [19].

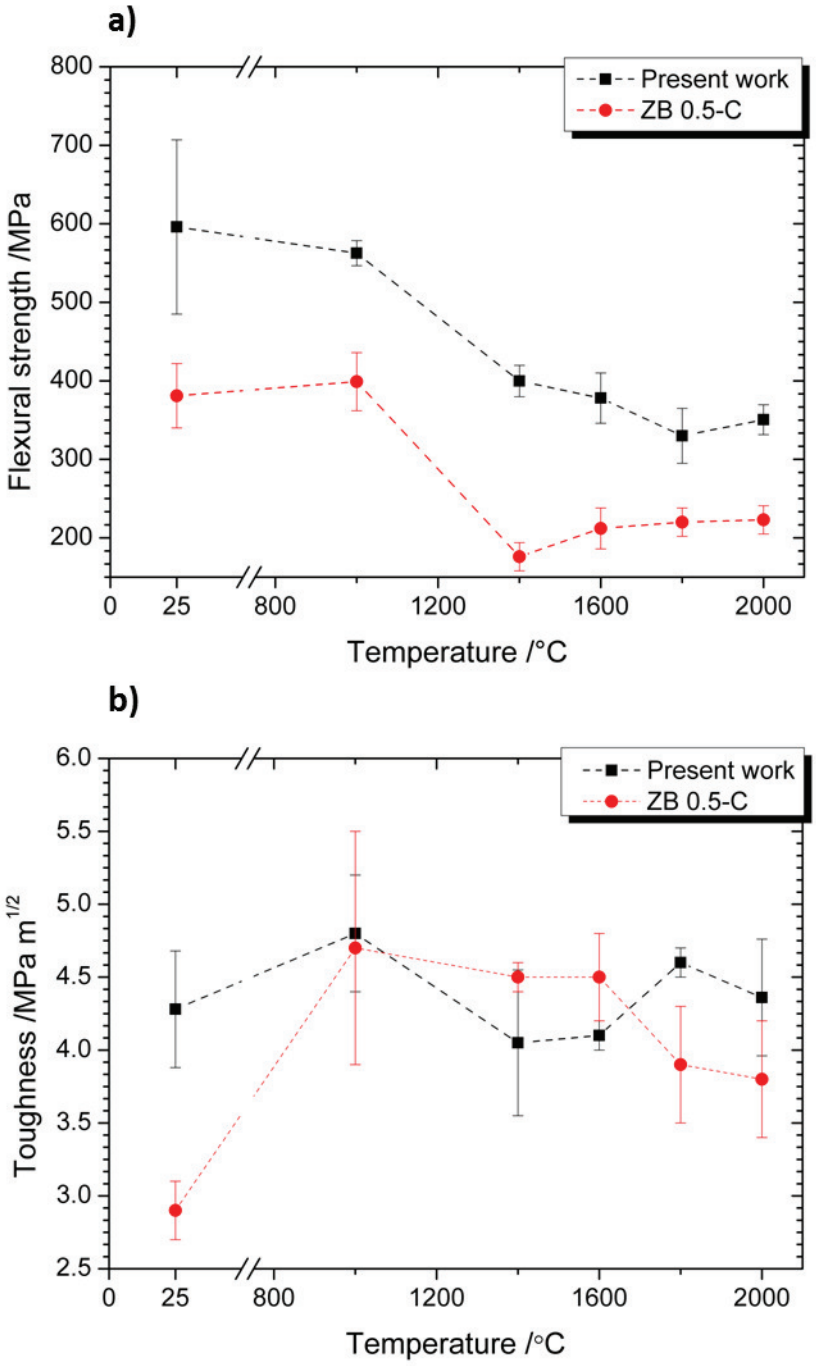

Figure 10. a) Flexure strength and b) fracture toughness for ZrB_2- 10 vol% ZrC as a function of temperature. Red circle symbols represent ZrB_2 with the addition of 0.5 vol% of carbon, which was used as reference material.

Neuman et al. [43] observed a similar trend for ZrB_2-10 vol% ZrC with a minimum value of the strength at 1600°C, even though the starting ZrC powder was coarser than in the present work. An additional mechanism leading to the strength degradation at 1400°C can be explained by the presence of the low-viscosity amorphous phase. The improved purity of the starting powders, and the low content of oxide phases, should not provoke any grain

boundary softening, which is typical, for example, of ZrO_2 [71]. Overall, addition of ZrC increased the strength of the ZrB_2 over the entire temperature range 25-2000°C. The strength decreased above 1000°C, but it is almost stable from 1600 to 2000°C, which is consistent with other reports of borides and carbides. Compared to room temperature, fracture toughness increased to ~4.8 MPa$\sqrt{m}$ at 1000°C, but decreased to a minimum of 4.1 MPa$\sqrt{m}$ at 1400°C and 1600°C. A similar observation was reported by Watts et al. [19] for ZrB_2-SiC ceramics, which was attributed to relaxation of the residual stresses occurring due to the mismatch in the CTE values. Fracture toughness increased to 4.6 MPa$\sqrt{m}$ at 1800°C and 4.4 MPa$\sqrt{m}$ at 2000°C, which were both higher than the value at room temperature. The increase of toughness in the range 1600-2000°C can be attributed to plasticity of ZrC since Neuman [60] observed a plateau in the toughness of ZrB_2 from 1500 to 2300°C. It should be noted, however, that in Neuman's work the grain size was >10 μm and this may have limited grain boundary sliding and, therefore, plasticity. The plasticity in the ZrC has been attributed to carbon self-diffusion by Lee et al. [30], who studied creep of single crystal $ZrC_{0.945}$ in the temperature range 1400-2000°C. They found that the activation energy for creep was comparable to the energy of carbon self-diffusion in single crystal $ZrC_{0.97}$, as reported by Sarian *et al* [35] and in polycrystalline $ZrC_{0.96}$ as reported by Babad-Zakhryapi [75]. These data support the hypothesis that dislocation motion is assisted by carbon diffusion and can be described with the model proposed by Kelly and Rowcliffe [39] for TiC that can be extended to all carbides with a NaCl structure [36]. This suggests that the addition of ZrC is effective in increasing the toughness not only at room temperature, as result of residual thermal stresses, but also at temperatures above 1600°C due to plasticity. Microstructures were examined before and after testing to find evidence of grain reorientation as a result of the stresses applied. As-sintered ZrB_2-ZrC ceramics did not exhibit any significant texturing or preferred orientation as indicated by the EBSD phase map as shown in Figure **11**. The distribution of ZrC within the ZrB_2 matrix appears to be homogeneous and no grain growth was observed after testing at elevated temperatures within the limit of the resolution of the EBSD map (0.5 μm). The grain size of the ZrB_2 was 3.2 ± 1.9 μm and 1.4 ± 0.8 μm for the ZrC and both had aspect ratios of 1.5 ± 0.5. These values are compatible with estimates made from the SEM images in Figure 1. Based on the inverse pole diagrams, no significant grain orientation was observed prior to testing at elevated temperatures.

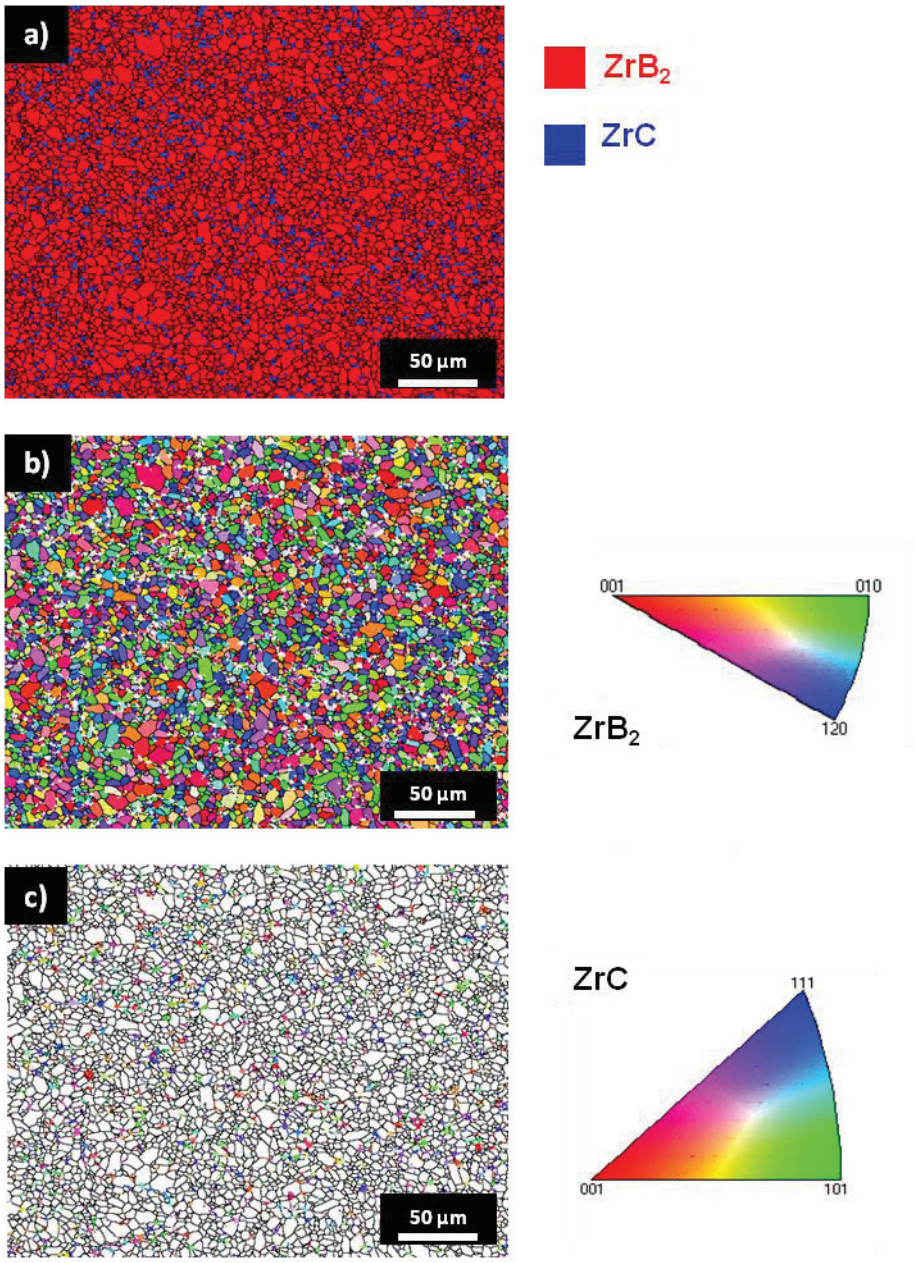

Figure 11. a) EBSD phase map of ZrB_2 - 10 vol% ZrC, b) Grain orientation for ZrB_2 and c) ZrC for the as-sintered ceramic.

EBSD mapping was conducted on the tensile and compressive surfaces of the specimens fractured at 1800°C and 2000°C. After testing at 1800°C, the degree of orientation of the grains was not noticeably changed; however, preferential orientation of ZrC grains occurred in a narrow band within 20 µm of the tensile surface of the specimen tested at 2000°C (Figure **12**). After testing, the grains were aligned with the <100> directions parallel to the tensile stress. No texturing was observed at any location more than ~20 µm from the tensile surface. It must be noted that this region has a slightly higher ZrC content (~1.3 vol%) than the bulk, which is consistent with the observation of carbothermal reduction of zirconia near the fracture surface.

Whilst ZrC grains became strongly oriented after testing at 2000°C, the ZrB_2 also showed a weak orientation of the [001] direction parallel to the tensile stress. Once again, this only occurred in proximity of the tensile surface.

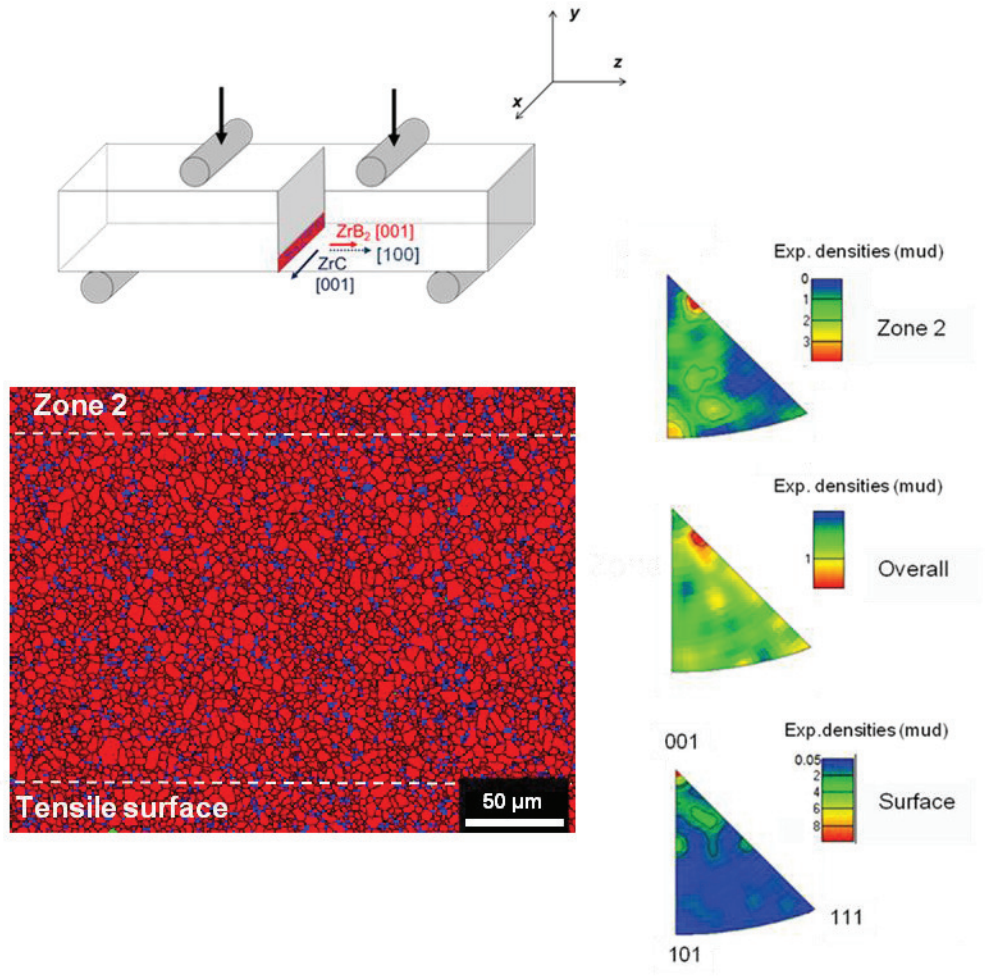

Figure 12. EBSD phase map of the tensile region of a specimen tested at 2000°C. ZrC is the red phase and ZrB_2 is blue. The inverse poles show the magnitude of the preferential orientation of ZrC grains in different areas along the x axis.

Figure **13** shows the evolution of the orientation for both the ZrB_2 and ZrC in the area close to the tensile surface. Following ASTM C1211, a relatively fast crosshead rate was used for testing at elevated temperature (4.0 mm min^{-1} at 2000°C) to maintain linear-elastic behavior. Previously, this degree of orientation has only been observed during long duration creep experiments when the strain rate is low [76]; it has not been observed before during fast fracture.

The orientation of ZrC may be the result of several mechanisms acting simultaneously. One possibility would be that plastic flow could produce orientation where the stress is high

enough, which could occur in a narrow region close to the tensile surface. However, the direction type of orientation observed in a face-centred cubic lattice such as ZrC should be $<-110>$ and not <100> [77]. A second possibility is that ZrC grains adjacent to the amorphous phase and ZrC formed by reduction of ZrO_2 can rotate and align along the <100> direction, which is the same orientation of the planar growth terraces in ZrC. Under an applied stress, which is maximized at the tensile surface, the terraces can rotate and align along the <100> direction. Another explanation is related to the cohesive strengths [78] of the ZrC/ZrC, ZrC/ZrB_2, ZrB_2/ZrB_2 and ZrC/amorphous phase interfaces, which is that grain ZrC rotation is observed at ZrC/ZrC and ZrC/viscous amorphous phase interfaces because the cohesive forces are lower than ZrB_2/ZrB_2 and ZrB_2/ZrC.

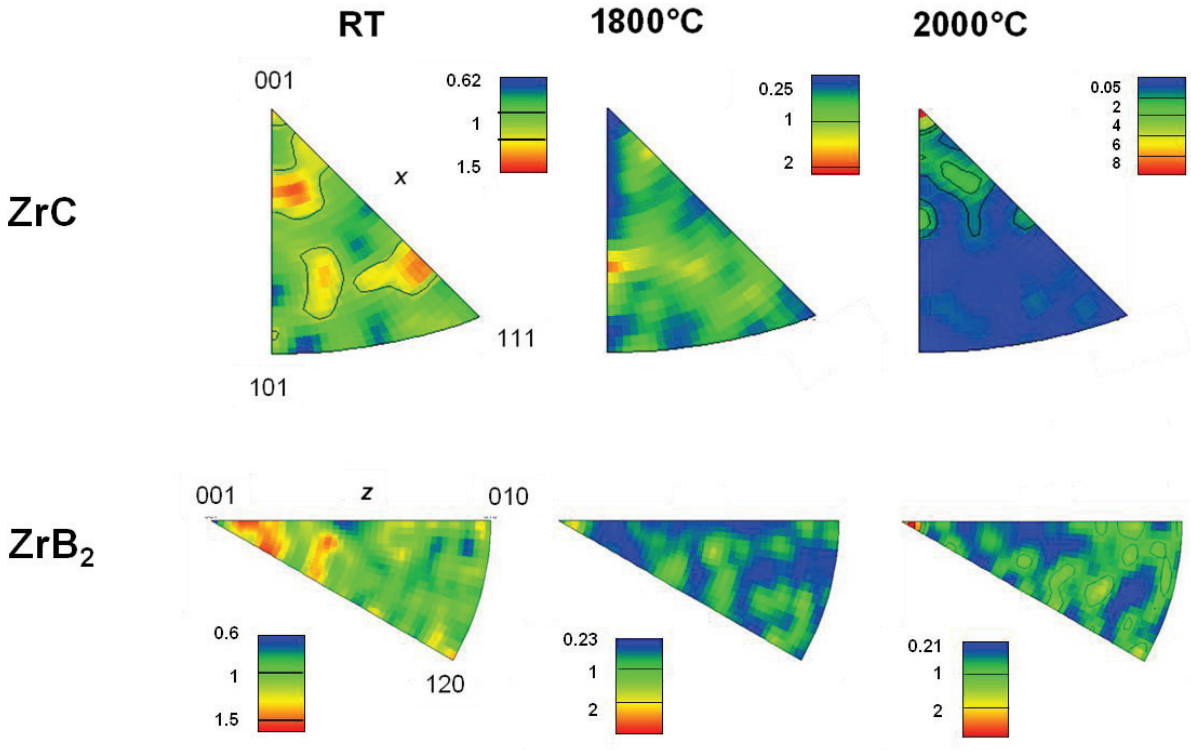

Figure 13. Orientation evolution with the testing temperature of ZrB_2 and ZrC grains on the tensile surface.

4. Conclusions

The mechanical behaviour of dense ZrB_2 - 10 vol% ZrC ceramics was studied from room temperature to 2000°C. The addition of 10 vol% ZrC particles into a ZrB_2 matrix enhanced the flexural strength over the entire range of temperatures compared to nominally pure ZrB_2. The strength of ZrB_2-10 vol% ZrC was nearly 600 MPa from room temperature up to 1000°C and it then decreased almost linearly with temperature to the minimum value of 330 MPa at 1800°C where it stabilized. The strength at 2000°C was 350 MPa, which is ~50% higher than

the strength of nominally pure ZrB_2 obtained by processing the same powders. Fracture toughness was 4.3 MPa$\sqrt{m}$ at room temperature and increased to 4.8 MPa$\sqrt{m}$ at 1000°C followed by a drop to 4.1 MPa$\sqrt{m}$ at 1400°C due to relaxation of residual thermal stresses. The toughness increased to 4.4 MPa$\sqrt{m}$ at 1800°C and above due to the possible plastic flow within the dispersed ZrC particles.

Microstructural analysis revealed that ZrC particles were both homogeneously distributed and randomly oriented in the as processed ZrB_2 matrix. In addition, a residual amorphous phase was observed adjacent to ZrC grains. Occasionally, zirconia grains were observed entrapped in the amorphous phase. For specimens fractured at 1800°C and below, ZrC grains on the fracture surface were randomly oriented. However, fracturing at 2000°C led to formation of terrace-like structures with well-defined crystallographic orientation and ZrC particles oriented with the <100> direction parallel to the tensile stress within 20 μm of the tensile surface of the specimens. At lower temperatures and away from the tensile surface at 2000°C, no texturing was observed. This is the first report of plastic deformation and texturing of ZrC during fast fracture.

Acknowledgements

This work was supported by Aerospace Materials for Extreme Environments program of the Air Force Office of Scientific Research (Grant number FA9550-14-1-0385 with program manager Ali Sayir) and the JECS Trust Foundation (Contract No. 201363-01)

Table 1. Microstructural, physical and mechanical properties of ZrB_2-ZrC ceramics at room temperature

Actual composition / vol%	Density / g cm^{-3}	Grain size / μm	Hardness / GPa	Modulus (static, dynamic) / GPa	Strength σ_b / MPa	Toughness K_{IC} / MPa$\sqrt{m}$	Critical flaw size (Y=1.59, 1.99) / μm
ZrB_2 = 89.9 ZrC = 9.9 C = 0.2	6.14	ZrB_2 4.7 ± 1.6 ZrC 1.7 ± 0.7	16.0 ± 0.2	525 ± 17 515 ± 1	596 ± 111	4.3 ± 0.5	20.4 13.0

Table 2. Mechanical properties of ZrB_2-ZrC ceramics at elevated temperature

Temperature / °C	Crosshead rate (strength, toughness) / mm/min	Strength σ_b / MPa	Toughness K_{IC} / MPa$\sqrt{m}$	Critical flaw size (Y=1.59 -1.99) / μm
1000	0.5, 0.03	563 ± 16	4.8 ± 0.4	28.8 – 18.4
1400	0.5, 0.04	400 ± 20	4.1 ± 0.5	40.6 – 25.9
1600	2.0, 0.05	378 ± 32	4.1 ± 0.1	46.5 – 29.7
1800	3.0, 0.05	330 ± 35	4.6 ± 0.1	76.6 – 49.1
2000	4.0, 0.06	350 ± 19	4.4 ± 0.4	61.2 – 39.1

References

1. Jackson, T., D. Eklund, and A. Fink, *High speed propulsion: Performance advantage of advanced materials.* Journal of materials science, 2004. **39**(19): p. 5905-5913.
2. Opeka, M., I. Talmy, and J. Zaykoski, *Oxidation-based materials selection for 2000 C+ hypersonic aerosurfaces: theoretical considerations and historical experience.* Journal of materials science, 2004. **39**(19): p. 5887-5904.
3. White, M.E. and W.R. Price, *Affordable hypersonic missiles for long-range precision strike.* Johns Hopkins APL technical digest, 1999. **20**(3): p. 415.
4. Wuchina, E., et al., *UHTCs: ultra-high temperature ceramic materials for extreme environment applications.* the electrochemical society interface, 2007. **16**(4): p. 30.
5. Fay, J.A., *Theory of stagnation point heat transfer in dissociated air.* Journal of the Aerospace Sciences, 1958. **25**(2): p. 73-85.
6. Mroz, C., *Zirconium diboride.* American Ceramic Society Bulletin, 1995. **74**(6): p. 164-165.
7. Toth, L., *Transition metal carbides and nitrides*. 2014: Elsevier.
8. Pierson, H.O., *Handbook of Refractory Carbides & Nitrides: Properties, Characteristics, Processing and Apps*. 1996: William Andrew.
9. Schuldies, J. and J. Branch, *Ceramic composites: emerging processes, applications.* Ceramic Industry, 1992. **138**(5): p. 43-46.
10. Fahrenholtz, W.G., et al., *Refractory diborides of zirconium and hafnium.* Journal of the American Ceramic Society, 2007. **90**(5): p. 1347-1364.
11. Monteverde, F., S. Guicciardi, and A. Bellosi, *Advances in microstructure and mechanical properties of zirconium diboride based ceramics.* Materials Science and Engineering: A, 2003. **346**(1–2): p. 310-319.

12. Sciti, D., et al., *Effect of different sintering aids on thermo–mechanical properties and oxidation of SiC fibers–Reinforced ZrB 2 composites.* Materials Chemistry and Physics, 2013. **137**(3): p. 834-842.
13. Sciti, D., et al., *Properties of a Pressureless-Sintered ZrB2–MoSi2 Ceramic Composite.* Journal of the American Ceramic Society, 2006. **89**(7): p. 2320-2322.
14. Sciti, D., et al., *Sintering and mechanical properties of ZrB2–TaSi2 and HfB2–TaSi2 ceramic composites.* Journal of the American Ceramic Society, 2008. **91**(10): p. 3285-3291.
15. Vasudévan, A.K. and J.J. Petrovic, *Proceedings of the First High Temperature Structural Silicides Workshop A comparative overview of molybdenum disilicide composites.* Materials Science and Engineering: A, 1992. **155**(1): p. 1-17.
16. Silvestroni, L., G. Meriggi, and D. Sciti, *Oxidation behavior of ZrB2 composites doped with various transition metal silicides.* Corrosion Science, 2014. **83**: p. 281-291.
17. Fahrenholtz, W.G., et al., *Pressureless sintering of zirconium diboride: particle size and additive effects.* Journal of the American Ceramic Society, 2008. **91**(5): p. 1398-1404.
18. Zhang, S., G. Hilmas, and W. Fahrenholtz, *Pressureless densification of zirconium diboride with boron carbide additions.* Journal of the American Ceramic Society, 2006. **89**(5): p. 1544-1550.
19. Watts, J., G. Hilmas, and W.G. Fahrenholtz, *Mechanical characterization of ZrB2–SiC composites with varying SiC particle sizes.* Journal of the American Ceramic Society, 2011. **94**(12): p. 4410-4418.
20. Monteverde, F., *Beneficial effects of an ultra-fine α-SiC incorporation on the sinterability and mechanical properties of ZrB2.* Applied Physics A, 2006. **82**(2): p. 329-337.
21. Tu, R., H. Hirayama, and T. Goto, *Preparation of ZrB2-SiC composites by arc melting and their properties.* Journal of the Ceramic Society of Japan, 2008. **116**(1351): p. 431-435.
22. Neuman, E.W., G.E. Hilmas, and W.G. Fahrenholtz, *Mechanical behavior of zirconium diboride–silicon carbide–boron carbide ceramics up to 2200 C.* Journal of the European Ceramic Society, 2015. **35**(2): p. 463-476.
23. Chamberlain, A.L., et al., *High-Strength Zirconium Diboride-Based Ceramics.* Journal of the American Ceramic Society, 2004. **87**(6): p. 1170-1172.
24. Zou, J., et al., *Strong ZrB2–SiC–WC ceramics at 1600° C.* Journal of the American Ceramic Society, 2012. **95**(3): p. 874-878.
25. Gropyanov, V. and L. Bel'tyukova, *Sintering and recrystallization of ZrC-ZrB2 compacts.* Soviet Powder Metallurgy and Metal Ceramics, 1968. **7**(7): p. 527-533.
26. Kats, S., S. Ordan'yan, and V. Unrod, *Compressive creep of alloys of the ZrC-ZrB2 and TiC-TiB2 systems.* Soviet Powder Metallurgy and Metal Ceramics, 1981. **20**(12): p. 886-890.
27. Tsuchida, T. and S. Yamamoto, *Spark plasma sintering of ZrB2–ZrC powder mixtures synthesized by MA-SHS in air.* Journal of materials science, 2007. **42**(3): p. 772-778.
28. Andrievskii, R., et al., *Effect of zirconium carbide and carbon additions on some physicomechanical properties of zirconium diboride.* Powder Metallurgy and Metal Ceramics, 1980. **19**(2): p. 93-94.
29. Darolia, R. and T. Archbold, *Plastic deformation of polycrystalline zirconium carbide.* Journal of Materials Science, 1976. **11**(2): p. 283-290.

30. Lee, D.W. and J.S. Haggerty, *Plasticity and Creep in Single Crystals of Zirconium Carbide.* Journal of the American Ceramic Society, 1969. **52**(12): p. 641-647.
31. Miloserdin, Y.V., et al., *The high-temperature creep of zirconium carbide.* Strength of Materials, 1972. **4**(3): p. 302-305.
32. Zubarev, P. and A. Shmelev, *Creep process kinetics and long-term strength of zirconium carbide. Communication 1.* Strength of Materials, 1980. **12**(2): p. 142-148.
33. Gridneva, I.V., et al., *Effect of temperature on the strength characteristics of zirconium carbide.* Soviet Powder Metallurgy and Metal Ceramics, 1976. **15**(8): p. 638-645.
34. Leipold, M.H. and T.H. Nielsen, *Mechanical Properties of Hot-Pressed Zirconium Carbide Tested to 2600°C.* Journal of the American Ceramic Society, 1964. **47**(9): p. 419-424.
35. Sarian, S. and J. Criscione, *Diffusion of carbon through zirconium monocarbide.* Journal of Applied Physics, 1967. **38**(4): p. 1794-1798.
36. Zubarev, P.V. and L.N. Dement'ev, *Relation between the activation energies of high-temperature creep and diffusion in transition metal carbides.* Strength of Materials, 1971. **3**(9): p. 1058-1061.
37. Miccioli, B.R. and P.T.B. Shaffer, *High-Temperature Thermal Expansion Behavior of Refractory Materials: I, Selected Monocarbides and Binary Carbides.* Journal of the American Ceramic Society, 1964. **47**(7): p. 351-356.
38. Lee, H.M. and L. Barbett, *Diffusion of carbon and uranium in uranium carbide.* Journal of Nuclear Materials, 1968. **27**(3): p. 275-284.
39. Kelly, A. and D. Rowcliffe, *Slip in titanium carbide.* physica status solidi (b), 1966. **14**(1): p. K29-K33.
40. Williams, W.S. and R. Schaal, *Elastic deformation, plastic flow, and dislocations in single crystals of titanium carbide.* Journal of Applied Physics, 1962. **33**(3): p. 955-962.
41. Hollox, G. and R. Smallman, *Plastic behavior of titanium carbide.* Journal of Applied Physics, 1966. **37**(2): p. 818-823.
42. Sarian, S., *Diffusion of carbon in TiC.* Journal of Applied Physics, 1968. **39**(7): p. 3305-3310.
43. Neuman, E.W., G.E. Hilmas, and W.G. Fahrenholtz, *Ultra-High Temperature Mechanical Properties of a Zirconium Diboride–Zirconium Carbide Ceramic.* Journal of the American Ceramic Society, 2015.
44. Kempter, C.P. and R. Fries, *Crystallographic Data. 189. Zirconium Carbide.* Analytical Chemistry, 1960. **32**(4): p. 570-570.
45. Neuman, E.W., et al., *Building an ultra-high-temperature mechanical testing system.* Testing and characterization of ceramics, 2013: p. 36.
46. Grathwohl, G., *Current testing methods—A critical assessment.* International Journal of High Technology Ceramics, 1988. **4**(2): p. 123-142.
47. Kempter, C.P. and R.J. Fries, *Crystallographic Data. 189. Zirconium Carbide.* Analytical Chemistry, 1960. **32**(4): p. 570-570.
48. Monteverde, F. and A. Bellosi, *Effect of the addition of silicon nitride on sintering behaviour and microstructure of zirconium diboride.* Scripta Materialia, 2002. **46**(3): p. 223-228.
49. Maitre, A. and P. Lefort, *Solid state reaction of zirconia with carbon.* Solid State Ionics, 1997. **104**(1): p. 109-122.
50. Ellingham, H., *Transactions and communications.* J. Soc. Chem. Ind.(London), 1944. **63**(5): p. 125.

51. Ebrahimi-Kahrizsangi, R. and E. Amini-Kahrizsangi, *Zirconia carbothermal reduction: Non-isothermal kinetics.* International Journal of Refractory Metals and Hard Materials, 2009. **27**(3): p. 637-641.
52. Réjasse, F., et al., *Experimental investigation and thermodynamic evaluation of the C–O–Zr ternary system.* RSC Advances, 2016. **6**(102): p. 100122-100135.
53. Song, M., et al., *Formation and growth mechanism of ZrC hexagonal platelets synthesized by self-propagating reaction.* Journal of Crystal Growth, 2008. **310**(18): p. 4290-4294.
54. Pimpinelli, A. and J. Villain, *Physics of crystal growth*. Vol. 19. 1998: Cambridge university press Cambridge.
55. Adamson, A.W. and A.P. Gast, *Physical chemistry of surfaces.* 1967.
56. Telle, R., L. Sigl, and K. Takagi, *Boride-Based Hard Materials.* Handbook of ceramic hard materials, 2000: p. 802-945.
57. Neuman, E., G. Hilmas, and W. Fahrenholtz, *Ultra High Temperature Mechanical Testing of ZrB2 Ceramics.* 2012.
58. Katoh, Y., et al., *Properties of zirconium carbide for nuclear fuel applications.* Journal of Nuclear Materials, 2013. **441**(1–3): p. 718-742.
59. Sciti, D., S. Guicciardi, and M. Nygren, *Spark plasma sintering and mechanical behaviour of ZrC-based composites.* Scripta Materialia, 2008. **59**(6): p. 638-641.
60. Neuman, E.W., *Elevated temperature mechanical properties of zirconium diboride based ceramics.* 2014.
61. Chawla, K.K., *Composite materials: science and engineering*. 2012: Springer Science & Business Media.
62. Aigner, K., et al., *Lattice parameters and thermal expansion of Ti (C x N 1− x), Zr (C x N 1− x), Hf (C x N 1− x) and TiN 1− x from 298 to 1473 K as investigated by high-temperature X-ray diffraction.* Journal of alloys and compounds, 1994. **215**(1): p. 121-126.
63. Chang, R. and L.J. Graham, *Low-temperature elastic properties of ZrC and TiC.* Journal of Applied Physics, 1966. **37**(10): p. 3778-3783.
64. Okamoto, N.L., et al., *Temperature dependence of thermal expansion and elastic constants of single crystals of ZrB 2 and the suitability of ZrB 2 as a substrate for GaN film.* Journal of applied physics, 2003. **93**(1): p. 88-93.
65. Taya, M., et al., *Toughening of a Particulate-Reinforced Ceramic-Matrix Composite by Thermal Residual Stress.* Journal of the American Ceramic Society, 1990. **73**(5): p. 1382-1391.
66. Le Roy, G., et al., *A model of ductile fracture based on the nucleation and growth of voids.* Acta Metallurgica, 1981. **29**(8): p. 1509-1522.
67. Houska, C., *Thermal expansion and atomic vibration amplitudes for TiC, TiN, ZrC, ZrN, and pure tungsten.* Journal of Physics and Chemistry of Solids, 1964. **25**(4): p. 359-366.
68. Krikorian, O.H., *Thermal expansion of high temperature materials*. 1960, California Univ., Livermore, CA (US). Lawrence Radiation Lab.
69. Shaffer, P.T. and M.D. Stanley, *Inert-Atmosphere Dilatometer for Use to 2000° C.* Journal of the American Ceramic Society, 1963. **46**(2): p. 104-106.
70. Touloukian, Y.S., et al., *Thermophysical Properties of Matter-the TPRC Data Series. Volume 13. Thermal Expansion-Nonmetallic Solids*. 1977, DTIC Document.
71. Rhodes, W.H., E.V. Clougherty, and D. Kalish, *Research and development of refractory oxidation-resistant diborides. Part II. Volume IV. Mechanical properties. Technical report, 15 September 1967--15 May 1969*. 1970, MANLABS, INC., CAMBRIDGE, MASS.

72. Neuman, E.W., G.E. Hilmas, and W.G. Fahrenholtz, *Strength of zirconium diboride to 2300° C.* Journal of the American Ceramic Society, 2013. **96**(1): p. 47-50.
73. Miracle, D.B. and H.A. Lipsitt, *Mechanical Properties of Fine-Grained Substoichiomebic Titanium Carbide.* Journal of the American Ceramic Society, 1983. **66**(8): p. 592-597.
74. Kharchenko, V.K., *High-temperature strength of refractory materials.* Strength of Materials, 1980. **12**(10): p. 1284-1294.
75. Babad-Zakhryapina, A., *22–27 July Int.* Atomic Energy Agency, Thermodynamics, Proc. Vienna, 1965. **2**: p. 172-180.
76. Bird, M.W., P.F. Becher, and K.W. White, *Grain rotation and translation contribute substantially to creep of a zirconium diboride silicon carbide composite.* Acta Materialia, 2015. **89**: p. 73-87.
77. Hull, D. and D.J. Bacon, *Chapter 3 - Movement of Dislocations*, in *Introduction to Dislocations (Fifth Edition)*. 2011, Butterworth-Heinemann: Oxford. p. 43-62.
78. Zhang, T., et al., *Compressive deformation behavior of a 30vol.% ZrC p/W composite at temperatures of 1300–1600° C.* Materials Science and Engineering: A, 2008. **474**(1): p. 382-389.